Accepted Manuscript

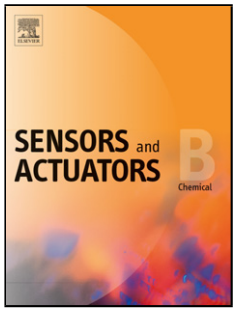

Title: Point-of-care Colorimetric Analysis through Smartphone Video

Authors: Benjamin Coleman, Chad Coarsey, Md Alamgir Kabir, Waseem Asghar

PII: S0925-4005(18)31990-7
DOI: https://doi.org/10.1016/j.snb.2018.11.036
Reference: SNB 25634

To appear in: *Sensors and Actuators B*

Received date: 27 April 2018
Revised date: 28 September 2018
Accepted date: 7 November 2018

Please cite this article as: Coleman B, Coarsey C, Alamgir Kabir M, Asghar W, Point-of-care Colorimetric Analysis through Smartphone Video, *Sensors and Actuators B: Chemical* (2017), https://doi.org/10.1016/j.snb.2018.11.036

This is a PDF file of an unedited manuscript that has been accepted for publication. As a service to our customers we are providing this early version of the manuscript. The manuscript will undergo copyediting, typesetting, and review of the resulting proof before it is published in its final form. Please note that during the production process errors may be discovered which could affect the content, and all legal disclaimers that apply to the journal pertain.

ACCEPTED MANUSCRIPT

Point-of-care Colorimetric Analysis through Smartphone Video

Benjamin Coleman[1,2], Chad Coarsey[1,2], Md Alamgir Kabir[1,2], Waseem Asghar[1,2,3,*]

[1]Asghar-Lab, Micro and Nanotechnology for Medicine, College of Engineering and Computer Science, Boca Raton, FL 33431

[2]Department of Computer & Electrical Engineering and Computer Science, Florida Atlantic University, Boca Raton, FL 33431

[3]Department of Biological Sciences, Florida Atlantic University, Boca Raton, FL 33431

* Corresponding Author's Email: wasghar@fau.edu

Graphical Abstract

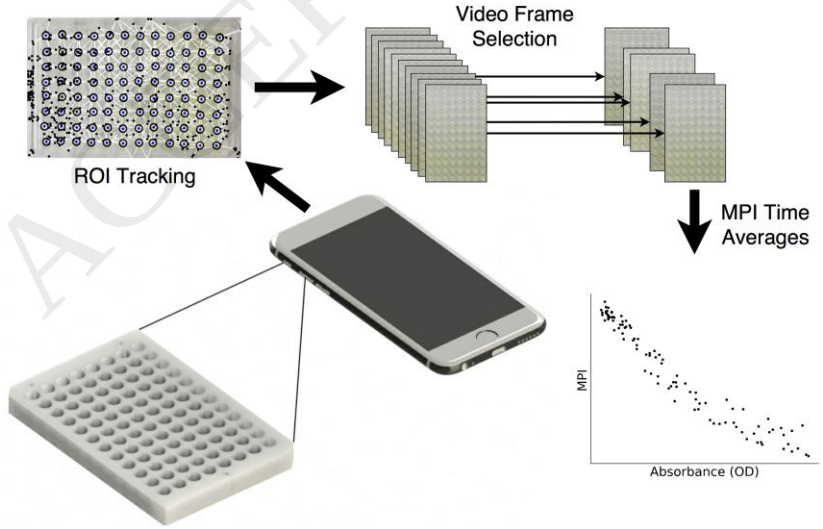

ACCEPTED MANUSCRIPT

ACCEPTED MANUSCRIPT

Highlights

- Smart-phone based diagnostic methods are being developed for disease detection.
- Existing assays require external smartphone hardware to obtain quantitative results.
- Development of a new method to record short video followed by feature extraction.
- Developed method enables point-of-care colorimetry with lower limit of detection.

Abstract

Point-of-care (POC) tests often rely on smartphone image methods for colorimetric analysis, but the results of such methods are frequently difficult to reproduce or standardize. The problem is aggravated by unpredictable image capture conditions, which pose a significant challenge when low limits of detection (LOD) are needed. Application-specific smartphone attachments are often used to standardize imaging conditions, but there has recently been an interest in equipment-free POC colorimetric analysis. Improved output metrics and preprocessing methods have been developed, but equipment-free imaging often has a high LOD and is inappropriate for quantitative tasks. Additional work is necessary to replace external smartphone attachments with algorithms. Towards this end, we have developed a video processing method that synthesizes many images into a single output metric. We use image features to select the best inputs from a large set of video frames and demonstrate that the resulting output values have a stronger correlation with laboratory methods and a lower standard error. The developed algorithm only requires 20 seconds of video and can easily be integrated with existing processing methods. We apply our algorithm to the NS1-based sandwich ELISA for Zika detection and show that the LOD is two times lower when our video-based method is used.

Keywords: Smartphone, Point of care, Biosensor, Zika Detection, Cell phone

ACCEPTED MANUSCRIPT

1. Introduction

A critical component of any point-of-care (POC) diagnostic system is the evaluation stage. Once a test for an analyte has been developed and can be practically administered under POC conditions, the test must also be evaluated with the same limitations. Conventional laboratory equipment is usually too infrastructure-dependent, bulky, or expensive to be well-suited to resource-constrained settings. This poses challenges for tests that require precise measurements, making the measurement system a limiting factor for POC detection and quantification.

Smartphones have been identified as a solution to the measurement problem because they are easily accessible and contain sophisticated sensors that can transmit data in real time from nearly anywhere in the world [1]. The smartphone camera has found applications in microfluidics [2], microscopy [3], and the evaluation of paper-based devices [4]. Since many assays produce a colorimetric response, cell phone imaging has emerged as a common method of smartphone-enabled POC evaluation. Quantitative colorimetric applications remain difficult to develop, but a wide variety of chemical and biological analytes can still be detected qualitatively. These include HIV [5] , tuberculosis [6], water-borne pathogens [7], environmental mercury contaminants [8] [9], chlorine concentrations [10], and trace quantities of explosive materials [11].

Smartphone cameras capture the image as a set of red, green, and blue (RGB) image channels, which must be processed to obtain a single output measurement. Regardless of the analyte, most analysis methods compute the mean pixel intensity (MPI) of the RGB channels within a region of interest (ROI) in the image. Some processing algorithms use colorspace transformation, while others use the RGB averages [12] [13] or function of RGB values [14]. In either case, the analysis depends on the existence of a relationship between RGB values and the concentration of an analyte. The method has shown good agreement with the absorbance readings from a visible-light spectrophotometer and is therefore useful

ACCEPTED MANUSCRIPT

for a wide range of bioanalytic applications [15]. Linear regression models have been used to calibrate the MPI response to an absorbance curve, with acceptable results under controlled conditions [16]. The regression model must have a sufficiently high correlation and low standard error in the target range for the MPI method to detect the target [17].

Unfortunately, imaging conditions can dramatically affect the validity of the analysis. If the image is taken at the wrong angle or the subject is out of focus, the analysis may fail. A variety of factors can interfere with the relationship between MPI values and the target. In some cases, the relationship may completely disappear. The readout can be compromised by reflections and glare [18], the separation distance and angle between the camera and sample, ambient light variations [19], the size of the ROI, and even the location of the ROI in the image [20]. Since smartphone cameras are optimized for consumer applications rather than scientific imaging, they apply automatic focusing and white-balance algorithms that complicate the problem [21].

This issue has already been addressed using smartphone attachments [22]. Such attachments provide constant illumination [18], standardize image capture conditions, and significantly improve the characteristics of the image [23] [24]. With high-quality input data, algorithms can achieve repeatable results and low limits of detection (LOD). Although attachment-free methods are more accessible and cost-effective, external equipment is often needed to meet performance specifications because equipment-free methods suffer from repeatability and standardization problems. To contend with methods that rely on hardware, they require advanced processing methods that are robust to image capture conditions and can handle low-quality input data.

Recent efforts have focused on the measurement challenges associated with equipment-free imaging [25]. It is desirable to eliminate the lighting box or attachment and replace it with better analysis methods, if possible. While lighting boxes and smartphone attachments are low-cost, they tend to be

ACCEPTED MANUSCRIPT

bulky, fragile and difficult to transport. Software, on the other hand, can be duplicated and distributed instantly at essentially no cost. Therefore, there has been a search for output metrics that are reliable under a wide variety of image capture conditions. The ROI median has been explored as an alternative to the MPI, as it is completely immune to limited amounts of discoloration [26]. MPI ratio metrics are extensively used to achieve a form of standardization between different imaging environments [10], and colorspace transformation has yielded good results for color-change assays [25]. The CIE 1931 chromaticity space [25], HSV hue channel [26] [27] [28], HSV saturation channel [29] [30] and grayscale intensity [15] have all been used as alternative metrics. These methods work because they combine the raw RGB values in ways that decouple the MPI from interfering factors [29]. Preprocessing algorithms have also been developed to reduce the effect of certain factors. For instance, a Fourier bias correction algorithm can remove the effect of uneven illumination at the expense of MPI dynamic range [31].

However, performance is still dependent on a variety of factors whose effects cannot be completely removed from single images using algorithms. Undesirable interference due to experimental conditions can cause snapshot-based results to be unpredictable. This factor has been identified as one of the most fundamental challenges for smartphone image-based colorimetric measurements [20]. Lighting boxes and smartphone attachments are indispensable because they remove detrimental factors from the algorithm input. However, the fact that specific problematic factors have been identified suggests that it may be possible to reliably differentiate between images that contain useful data and those that do not, even when a lighting box is not used. Given a large set of images, a classification algorithm could act as a virtual light box and select the best inputs for the processing algorithm, improving the quality of results when specialized equipment is not available. More importantly, this method could reject images with bad capture conditions. Such an algorithm would also be able to provide users with instant feedback on the measurement, allowing them to improve conditions if needed.

ACCEPTED MANUSCRIPT

To the best of our knowledge, smartphone videos have not been considered for this purpose, even though they offer the ability to collect a large set of high-resolution images. Smartphone videos have been used to measure the rate of a chemical reaction, but have not been applied to tests that require a single measurement [32]. However, video data includes temporal information about imaging conditions, allowing time-dependent variations to be identified even for single endpoint measurements. Furthermore, analysis of a large collection of images may be more accurate than the unpredictable results of single image analysis. Here, we investigate the use of smartphone video to obtain the best possible set of input data. We track the correlation and standard error of a typical calibration dataset over several thousand video frames and examine the factors that influence performance. In addition, we develop image features that can identify problematic image capture conditions. We use the features in a classification algorithm to reject low-quality input frames and we show that the algorithm can halve the LOD of a smartphone evaluation scheme for the NS1-based Zika sandwich ELISA.

2. Materials and Methods

2.1 Data Collection

Calibration data for modeling and feature engineering was obtained using serial dilutions of an HRP-antibody conjugate. Specifically, anti-HIV-1 p24 antibody was conjugated with horseradish peroxidase (HRP) and serially diluted in a standard 96-well plate. Absorbance values were measured using a spectrophotometer (Molecular Devices) at the 450 nm wavelength to obtain a gold standard measurement method for data modeling purposes.

We recorded images and videos of the 96 well plate using the iPhone 6S camera and the default camera app. The resolution of the images and videos were both set to the ultra-high 4K resolution option (2448x3264). We captured images and videos according to established guidelines for the image capture conditions [31]. Videos were also recorded under a wide range of conditions. We included frames taken

ACCEPTED MANUSCRIPT

at angles ranging from 45 degrees to 90 degrees, and we obtained frames at a variety of distances to the sample. We introduced automatic white-balancing and blur by refocusing the image to an area away from the 96 well plate. In all, we captured 14 images and 10 videos comprising 7,635 video frames at 60 frames per second (FPS). The videos were processed using a custom video frame classification and analysis algorithm (Figure 1).

2.2 Video ROI Extraction and Tracking

The 96 ROIs (one ROI per well) were manually tagged on a computer using a custom cross-platform analysis program implemented with Python and OpenCV. The program offers a user-friendly GUI, and a skilled user can mark all 96 ROIs in under a minute. This method can easily be extended to a smartphone interface that allows the user to tap on ROI centers, with no loss of functionality. Automatic extraction methods are also possible using colored templates or special markings on the plate.

However, it is impractical to manually extract ROIs from each frame. A 5 second video at 60 FPS will have 300 frames, requiring over two hours of manual data entry. Likewise, automatic ROI extraction may be too expensive to compute for each frame on the smartphone. Therefore, we developed an algorithm to track ROIs from frame to frame throughout the video, given a set of initial coordinates.

We used Shi-Tomasi corner detection to obtain a set of corner points, and we computed the Lucas-Kanade optical flow for each point. Each frame of the video, we updated the location of the ROI centers using the ten nearest corner points. Using the sparse optical flow of the image, we found the distance each corner point had traveled since the previous frame. We moved the ROI center by the mean displacement of the ten nearest corner points. Although the method worked well for short videos, the ROI centers began to drift after several hundred frames and for fast-moving video content. Therefore, we also manually updated the ROI center locations when necessary. Using OpenCV, we overlaid the

ACCEPTED MANUSCRIPT

video with the ROI boundaries to ensure that there was no drift and that the algorithm correctly extracted the 96 wells for all video frames.

2.3 Frame Features

We developed a set of image features to identify and reject blurred images, images with excessive white-balancing, and images that may have other issues including glare and reflection. Features were designed manually rather than with automatic statistical or machine learning methods. We designed the features to detect imaging conditions that previous studies have identified as problematic [18] [19] [31].

2.3.1 Laplacian Blur Metric

We rejected images where the ROIs were out of focus because the signals from adjacent ROIs can overlap in a blurry image. Blurred images also pose problems for ROI extraction and for the ROI tracking algorithm. Problematic images can be identified using the variance of the Laplacian of the image [33], which we refer to as the Laplacian blur metric (LBM). If the image has no sharp edges and is out of focus, then the Laplacian blur metric will be low (LBM < 10). Higher blur metric values indicate a sharper image. We computed this feature only for the area of the image occupied by the 96 well plate. Other undesirable parts of the image may be in focus even when the 96 ROIs are not, artificially raising the variance of the Laplacian.

2.3.2 ROI Variance

To detect images with glare, reflections, or suboptimal ROIs, we considered the pixel intensity variance as a feature. Glare and reflections can cause part of the ROI to be discolored and have abnormally high intensity, while off-center ROIs contain pixels from regions of the image that should not be measured. Images taken at an oblique angle often include undesirable refractions from edges of the microfluidic chip, 96 well plate, or POC device.

ACCEPTED MANUSCRIPT

When included in a ROI, glare and reflections introduce multimodality, increase the range of pixel values, and artificially shift the MPI value. These features will therefore increase the variance of the pixel intensity histogram within the ROI. We computed the maximum variance of all ROIs in a frame for the ROI variance feature.

2.3.3 First Difference of the MPI

Automatic white-balancing causes a vertical shift in pixel intensity values, making it difficult to compare MPI values from image to image. Images that are improperly white balanced will require bias correction and the results will suffer from a reduced dynamic range [31]. Image burning effects, where the image appears washed-out and the dynamic range is affected, have also been reported due to glare and improper white balance conditions [18]. To detect issues with white balancing, we took the first difference of the blue MPI over time. If the MPI values in one frame have changed significantly since the previous frame, then magnitude of the first difference will be large.

2.3.4 ROI Analysis

For the Anti-HIV-1 p24 dataset, we captured images and videos under diffuse indoor lighting provided by white fluorescent overhead lights. We analyzed the images with the MPI of the RGB blue image channel. This value is computed as the arithmetic mean of all pixel intensities in the blue channel of the ROI. MPI and absorbance have an established linear relationship for sufficiently small absorbance values (OD < 1), which is also the most common absorbance range for bioanalytic applications [16]. Therefore, we performed linear regression to determine the relationship between the 96 MPI values and the SpectraMax spectrophotometer (Molecular Devices) output at 450 nm for each image and video frame. We computed the Pearson product moment correlation coefficient and the standard error of the regression line for each frame.

ACCEPTED MANUSCRIPT

We also computed the image features for each frame to investigate relationships between the features and quality of the calibration data. We rejected frames with a low blur metric (LBM < 10) and high ROI variance to obtain a high-quality subset of the video frames. The blur threshold was found by noting the point at which manual ROI identification became difficult. For the variance threshold, we rejected frames with a value greater than 25% of the maximum variance in the entire video. We found 96 MPI time averages by computing the mean of the MPI values from all selected frames. Since the sample sizes of each ROI were the same, the time average is equivalent to the grand mean of all pixel values within the ROI for every frame. We also found the 96 ROI time averages for the entire video, for comparison and to determine whether frame averages can improve performance.

2.3.5 Algorithm Validation

To demonstrate the practical applications of our system, we evaluated the standard Zika NS1-based sandwich ELISA with the smartphone algorithm. The ELISA procedure runs to completion in under 2 hours. The full procedure, including sample preparation, is as follows.

Mouse anti-Zika NS1 monoclonal antibody (BioFront Technologies) was diluted 2 µg/mL concentration in carbonate/bicarbonate buffer (pH 9.6) and incubate overnight at 4^{o} C after adding on a 100ul on each well on a 96 well plate (Greiner cellstar). After 3x washing with PBS (pH 7.4) the plate was blocked with 200 ul of SuperBlock™ T20 (TBS) blocking buffer (Thermofisher) on each well and again incubated overnight at 4 o C. 100 ul of different concentration of ZIKV NS1 antigen (BioFront Technologies) and control was added after 3x rinsing with PBS (pH 7.4) and incubated at room temperature for 2 hours. 100ul of HRP-labeled Anti-Zika NS1 monoclonal antibody (BioFront Technologies) diluted (1:1000) in PBST+3% BSA was added on each well, incubated for 1 hour at room temperature followed by 3x washing with the PBS (pH 7.4). 100 uL TMB (Thermofisher) was added and waited until the blue color was generated and the reaction was stopped by adding H_2SO_4. The OD values were obtained using

ACCEPTED MANUSCRIPT

SpectraMax microplate readers (Molecular Devices) at a wavelength of 450 nm. Smartphone images and videos were obtained using the iPhone 6 under a variety of lighting conditions. In addition to the fluorescent overhead lighting in the lab, images and videos were also captured outdoors under completely uncontrollable imaging conditions. The limit of detection for the NS1 protein was computed using the standard deviation of the blanks, with a sufficiently large number of frames ($n > 500$).

3 Results

We prepared a 96 well plate with multiple dilutions and imaged it using a smartphone. No external equipment was used, and we captured images and videos under a wide range of image capture conditions (Figure 1). We found that imaging conditions to analyze the colorimetric assays can vary even over the course of a few seconds of video, adversely affecting our MPI analysis. We observed an improvement in performance when we used the average from multiple frames, with an additional improvement from our frame selection algorithm.

Even when images visually appear similar, MPI analysis can yield substantially different results. Figure 2 illustrates that two images taken under similar conditions can have different MPI analyses. Images A and B were taken under the same lighting conditions but with different separating distances to the plate. The standard errors are approximately the same, but the dynamic range and correlation from Image B are nearly double the range and correlation from Image A (Figure 2). A dynamic view of this behavior can be found in Supplementary Videos 1 and 2, which overlays the correlation, standard error, and scatter plot on top of the ROI extraction video.

The Laplacian blur metric (LBM) and peak ROI variance had a clear association with the correlation and standard error of the regression line for each frame. Figure 3 shows a plot of our image features and the MPI analysis parameters over time. Video A was taken without interference, while video B was subjected to white-balancing and blur. We induced these effects by refocusing the camera away from

ACCEPTED MANUSCRIPT

the 96 well plate after one, five, and nine seconds of video. For the first 16 seconds of video A, the camera was moved vertically toward and away from the plate. The remainder of video A was taken under approximately constant conditions.

In both videos, changes in variance and LBM were associated with changes in the correlation coefficient. The ROI variance increased within the majority of the 96 wells for substandard imaging conditions (Figure 4). The first difference also had a relationship with the predicted video characteristic, with peaks that aligned with the white-balance and blur events in video B (Figure 3). Such events were not present in video A, where the first difference had a relatively small absolute value. Dynamic range was also an important difference between video A and video B. The frames with the highest correlation in video A had an MPI range of 60, while the highest correlated frames from video B had an MPI range of 45.

Figure 5 shows the results of our classification algorithm with video A (top), video B (middle), and a third video taken with an off-center 96 well plate (bottom). Although some frames were improperly classified, the algorithm typically selected frames with the highest correlation and lowest standard error. In video A, accepted frames (n = 1225) had an average R^2 of 0.92 (s = 0.02) while rejected frames (n = 1038) had an average R^2 of 0.85 (s = 0.03). For video B, acceptances (n = 50) had an average R^2 of 0.87 (s = 0.05) while the rejections (n = 623) had an average R^2 of 0.31 (s = 0.26).

The set of 96 time-averaged ROIs had a higher correlation than the set of 96 ROIs from most of the individual video frames (Figure 5). Two sets of frames were used to compute the time-averaged MPIs: the entire set of frames and the set of selections from the classification algorithm. Although the selected frame set did perform better in all tests, the difference was small for videos without white balance or blur issues. However, videos with blurry conditions benefitted significantly from the classification algorithm. The correlations of the time-averaged MPIs are shown as dashed red lines in Figure 5.

ACCEPTED MANUSCRIPT

Because the time-averaged MPIs outperformed most of the individual frames in terms of standard error, we investigated the distribution of MPI values over time. We found that MPI values were not constant throughout the video, even for constant imaging conditions. Instead, the MPI values from each frame form a distribution with a central tendency, offering one possible explanation for the performance improvement when using time-averaged MPI values.

The frame selection step also improved performance, particularly for unpredictable image capture conditions (Figure 6). The MPI value from a single well of the 96-well plate can change dramatically over the course of an entire video, resulting in a relatively high LOD of 35.5 ng/ml for the NS1-based sandwich ELISA. When the frame selection algorithm is used, the LOD drops to 16 ng/ml. The MPI values from each video frame do exhibit a central tendency, but variable image capture conditions introduce outliers, resulting in a high interquartile range (IQR) when the classification algorithm is not used. The IQR of the classifier output is nearly four times lower for unpredictable conditions but remains the same under constant fluorescent indoor lighting. The IQR is represented as the height of the shaded box, and the decrease in variance can be seen directly from the boxplots in Figure 6. It is important to note that the error bars in Figure 6 represent the 2^{nd} and 98^{th} percentile of the data and that 50% of the results lie within the box.

4 Discussion

We found that the correlation, standard error, and range of the response are directly affected by factors during image capture, even for images that are taken under similar conditions and look the same. Since these parameters are directly related to the LOD and quantification performance, MPI analysis suffers from repeatability and standardization issues. In some cases, the correlation between OD and MPI can drop to minimal levels and the range of the response can vary by a factor of two (Figure 2). Performance problems can be caused by changes in experimental conditions, such as background light intensity,

ACCEPTED MANUSCRIPT

distance from the phone to the sample (Figure 4), position of the camera (Figure 5C), and camera settings such as white balance and blur (Figure 3B). It is particularly important to center the image on the sample and the ROIs on the wells of the 96 well plate (Figure 5C). However, we found that single snapshot images can be unreliable even when taken under the same environmental conditions with conditions such as camera position, settings, and angle held constant (Figure 2).

We found that problematic input data can be detected using features of the image. Our blur metric, based on the Laplacian of the image, successfully rejects frames where the 96 well plate is out of focus. The first difference of MPI values over time can identify time instances in the video when white balancing occurs or when illumination conditions change. The peak ROI variance is an indicator of measurement quality, since low-variance ROIs tend to produce calibration results with high correlation and low standard error.

Using these features, the classification algorithm can detect and reject conditions that interfere with the optical density measurement. The feature-based algorithm is attractive because it does not require prior knowledge of the calibration result or spectrophotometer readout. The method enables image capture apps that provide immediate user feedback during data collection and apps that automatically detect when a good measurement can be made. The use of high-quality input data results in an increase in the correlation of the calibration curve and a reduction in standard error.

Even small improvements in correlation and standard error can have a significant impact on LOD and quantification performance of any diagnostic assay. MPI analysis is usually studied as an alternative to conventional spectrophotometric or colorimetric methods. The relationship between MPI and absorbance is important for later clinical studies [34]. When the analysis is finally tested for a particular application, statistical tools such as Bland-Altman plots or residual plots will likely be used to determine the agreement between MPI analysis and accepted methods. High correlation and low standard error

ACCEPTED MANUSCRIPT

are a necessary but insufficient condition for good agreement between measures. Low standard error is also important for the calibration of quantitative applications. If inferior input data weakens the relationship MPI and absorbance, practical applications may encounter measurement problems.

The MPI time-averages perform very well, with correlation and standard error parameters that are better than most individual video frames and images. When the classification algorithm is used, the correlation of the MPI time-average is among the highest of the component video frames and the standard error is minimized (Figure 5). Interestingly, the classification algorithm may not be needed to improve the results when lighting conditions are constant. For videos without serious blur or white balance issues, the MPI time-average of all frames had a satisfactory performance (Figure 5C). This can be explained because the MPI values exhibit random time variations with a central tendency. By computing the time-average of MPIs from many frames, we obtain an output that is close to this central tendency. A sufficiently large number of frames can, in many cases, be gathered by the smartphone camera in under 20 seconds.

However, the classification algorithm substantially improves performance for unpredictable capture conditions. The method works by selecting images that have similar capture conditions, which reduces the variance at each concentration. When the method was applied to a standard sandwich ELISA for the Zika virus, the algorithm substantially improved the LOD over existing single-image methods (Figure 6). Single-image analysis would produce results analogous to the results from all frames in Figure 6, since this plot shows the response for many single video frames. The classifier improves the measurement process because it rejects snapshots that are likely to produce outliers. When the input was filtered by the classification algorithm, the LOD dropped from 35.5 ng/ml to 16 ng/ml (Figure 6). It is important to note that there are bias and dynamic range differences between the indoor and outdoor environments in Figure 6. Although the algorithm does not standardize measurements from different imaging environments, it does reduce the variance of multiple measurements taken under the same conditions.

ACCEPTED MANUSCRIPT

To standardize measurements between environments, existing calibration strips [4] [19] or white balance correction algorithms may be used [31] [32].

Another important consideration is the sensitivity and selectivity of the Zika NS1-based sandwich ELISA when evaluated using MPI values. The sensitivity and selectivity are provided by BioFront Technologies for the case when the assay is evaluated by absorbance measurements from a plate reader. Unfortunately, it is only possible to approximate absorbance using MPI values. Therefore, the sensitivity and selectivity will necessarily be lower when the assay is evaluated using our method. The analytic sensitivity, defined in terms of the smallest detectable concentration of NS1, increases when the algorithm is used because the variance of the measurement decreases (Figure 6). In this context, the selectivity of our method is its ability to determine Zika NS1 protein concentrations without interference from environmental conditions, lighting noise, and other factors. Since concentration can be predicted by absorbance using the standard curve and there is high selectivity of the Zika assay when evaluated with absorbance, we may approximate the selectivity of our method as the amount of variation in MPI that is due to changes in absorbance. The interpretation of the R^2 value is the percentage of the MPI response that can be explained by changes in absorbance. Therefore, the selectivity of our method is approximately the R^2 value of the absorbance-MPI curve. For the indoor Zika assay this value was 0.75 and for the outdoor assay the R^2 value was 0.69. Therefore, our algorithm improves selectivity by improving the R^2 correlation between MPI and absorbance and it improves sensitivity by reducing the standard error of the estimate, which decreases the LOD.

Video methods are not currently prevalent in the literature, but they merit further exploration for bioanalytical applications because they offer a wealth of information about imaging conditions. Our classification method exploits this information to filter out variations in image capture conditions from the input data. Since the frame selection method acts as a preprocessing technique, it can be used with any existing processing algorithm. Although we used the most common form of MPI analysis, the

ACCEPTED MANUSCRIPT

classifier output could have been fed into systems that perform colorspace transformation, correct white balance, standardize ambient lighting variations, or use calibration strips. Regardless of the processing technique, high-quality inputs will improve the characteristics of the output. By imposing restrictions on video frame quality, our algorithm selects the best possible set of input images and acts as the software equivalent of a smartphone attachment.

5 Conclusion

Smartphone algorithms for diagnostic assays frequently suffer from variable lighting and image conditions. The variability can be introduced by environmental factors or by user error during assay imaging and analysis. We developed a video processing method to improve the repeatability of POC MPI analysis. We demonstrated that it is possible to reject low-quality input data using image features. Using these features in a classification algorithm, we selected high-quality frames and achieved an improvement in correlation and standard error for the MPI-absorbance relationship. When the method was applied to an ELISA assay for Zika, it substantially reduced the limit of detection under realistic POC imaging conditions. The method is generally applicable to any smartphone imaging method that uses an output parameter to estimate a colorimetric change. The developed video method is easy to integrate with other processing techniques, since it acts as a preprocessing and post-processing step. Existing algorithms can be applied to each frame and used to obtain the output value without any modification. We believe that video analysis can improve measurement performance for a wide range of POC tests and lead to more user-friendly measurement applications.

ACCEPTED MANUSCRIPT

Acknowledgements

ACCEPTED MANUSCRIPT

We acknowledge research support from Florida Department of Health (FDOH) 7ZK10, NIH R15AI127214, Institute for Sensing and Embedded Networking Systems Engineering (I-SENSE) Research Initiative Award, FAU Faculty Mentoring Award, Humanity in Science Award, and a start-up research support from College of Engineering and Computer Science, Florida Atlantic University, Boca Raton, FL.

Conflict of Interests

The authors declare no conflict of interest.

ACCEPTED MANUSCRIPT

ACCEPTED MANUSCRIPT

References

[1] S. K. Vashist, P. B. Luppa, L. Y. Yeo, A. Ozcan and J. H. T. Luong, "Emerging technologies for next-generation point-of-care testing," *Trends in biotechnology,* vol. 33, pp. 692-705, 2015.

[2] S. Wang, X. Zhao, I. Khimji, R. Akbas, W. Qiu, D. Edwards, D. W. Cramer, B. Ye and U. Demirci, "Integration of cell phone imaging with microchip ELISA to detect ovarian cancer HE4 biomarker in urine at the point-of-care," *Lab on a Chip,* vol. 11, pp. 3411-3418, 2011.

[3] H. Zhu, I. Sencan, J. Wong, S. Dimitrov, D. Tseng, K. Nagashima and A. Ozcan, "Cost-effective and rapid blood analysis on a cell-phone," *Lab on a Chip,* vol. 13, pp. 1282-1288, 2013.

[4] N. R. Pollock, J. P. Rolland, S. Kumar, P. D. Beattie, S. Jain, F. Noubary, V. L. Wong, R. A. Pohlmann, U. S. Ryan and G. M. Whitesides, "A paper-based multiplexed transaminase test for low-cost, point-of-care liver function testing," *Science translational medicine,* vol. 4, pp. 152ra129--152ra129, 2012.

[5] H. Shafiee, S. Wang, F. Inci, M. Toy, T. J. Henrich, D. R. Kuritzkes and U. Demirci, "Emerging technologies for point-of-care management of HIV infection," *Annual review of medicine,* vol. 66, pp. 387-405, 2015.

[6] B. Veigas, J. M. Jacob, M. N. Costa, D. S. Santos, M. Viveiros, J. In{\'a}cio, R. Martins, P. Barquinha, E. Fortunato and P. V. Baptista, "Gold on paper--paper platform for Au-nanoprobe TB detection," *Lab on a Chip,* vol. 12, pp. 4802-4808, 2012.

[7] H. Zhu, O. Yaglidere, T.-W. Su, D. Tseng and A. Ozcan, "Cost-effective and compact wide-field fluorescent imaging on a cell-phone," *Lab on a Chip,* vol. 11, pp. 315-322, 2011.

[8] G.-H. Chen, W.-Y. Chen, Y.-C. Yen, C.-W. Wang, H.-T. Chang and C.-F. Chen, "Detection of mercury (II) ions using colorimetric gold nanoparticles on paper-based analytical devices," *Analytical chemistry,* vol. 86, pp. 6843-6849, 2014.

[9] Q. Wei, R. Nagi, K. Sadeghi, S. Feng, E. Yan, S. J. Ki, R. Caire, D. Tseng and A. Ozcan, "Detection and spatial mapping of mercury contamination in water samples using a smart-phone," *ACS nano,* vol. 8, pp. 1121-1129, 2014.

[10] S. Sumriddetchkajorn, K. Chaitavon and Y. Intaravanne, "Mobile device-based self-referencing colorimeter for monitoring chlorine concentration in water," *Sensors and Actuators B: Chemical,* vol. 182, pp. 592-597, 2013.

[11] M. O. Salles, G. N. Meloni, W. R. Araujo and T. R. L. C. Paixao, "Explosive colorimetric discrimination using a smartphone, paper device and chemometrical approach," *Analytical Methods,* vol. 6, pp. 2047-2052, 2014.

[12] C. M. McGeough and S. O'Driscoll, "Camera phone-based quantitative analysis of C-reactive protein ELISA," *IEEE transactions on biomedical circuits and systems,* vol. 7, pp. 655-659, 2013.

[13] A. J. S. McGonigle, T. C. Wilkes, T. D. Pering, J. R. Willmott, J. M. Cook, F. M. Mims and A. V. Parisi, "Smartphone Spectrometers," *Sensors,* vol. 18, p. 223, 2018.

ACCEPTED MANUSCRIPT

[14] R. C. Murdock, L. Shen, D. K. Griffin, N. Kelley-Loughnane, I. Papautsky and J. A. Hagen, "Optimization of a paper-based ELISA for a human performance biomarker," *Analytical chemistry,* vol. 85, pp. 11634-11642, 2013.

[15] T. Ogirala, A. Eapen, K. G. Salvante, T. Rapaport, P. A. Nepomnaschy and A. M. Parameswaran, "Smartphone-based colorimetric ELISA implementation for determination of women's reproductive steroid hormone profiles," *Medical \& biological engineering \& computing,* vol. 55, pp. 1735-1741, 2017.

[16] B. Berg, B. Cortazar, D. Tseng, H. Ozkan, S. Feng, Q. Wei, R. Y.-L. Chan, J. Burbano, Q. Farooqui, M. Lewinski and others, "Cellphone-based hand-held microplate reader for point-of-care testing of enzyme-linked immunosorbent assays," *ACS nano,* vol. 9, pp. 7857-7866, 2015.

[17] J. M. Bland and D. G. Altman, "Comparing methods of measurement: why plotting difference against standard method is misleading," *The lancet,* vol. 346, pp. 1085-1087, 1995.

[18] S. C. Kim, U. M. Jalal, S. B. Im, S. Ko and J. S. Shim, "A smartphone-based optical platform for colorimetric analysis of microfluidic device," *Sensors and Actuators B: Chemical,* vol. 239, pp. 52-59, 2017.

[19] L. Shen, J. A. Hagen and I. Papautsky, "Point-of-care colorimetric detection with a smartphone," *Lab on a Chip,* vol. 12, pp. 4240-4243, 2012.

[20] K. E. McCracken and J.-Y. Yoon, "Recent approaches for optical smartphone sensing in resource-limited settings: a brief review," *Analytical Methods,* vol. 8, pp. 6591-6601, 2016.

[21] A. Roda, E. Michelini, M. Zangheri, M. Di Fusco, D. Calabria and P. Simoni, "Smartphone-based biosensors: A critical review and perspectives," *TrAC Trends in Analytical Chemistry,* vol. 79, pp. 317-325, 2016.

[22] O. Mudanyali, S. Dimitrov, U. Sikora, S. Padmanabhan, I. Navruz and A. Ozcan, "Integrated rapid-diagnostic-test reader platform on a cellphone," *Lab on a Chip,* vol. 12, pp. 2678-2686, 2012.

[23] S. K. Vashist, T. Oordt, E. M. Schneider, R. Zengerle, F. Stetten and J. H. T. Luong, "A smartphone-based colorimetric reader for bioanalytical applications using the screen-based bottom illumination provided by gadgets," *Biosensors and Bioelectronics,* vol. 67, pp. 248-255, 2015.

[24] S. Sumriddetchkajorn, K. Chaitavon and Y. Intaravanne, "Mobile-platform based colorimeter for monitoring chlorine concentration in water," *Sensors and Actuators B: Chemical,* vol. 191, pp. 561-566, 2014.

[25] A. K. Yetisen, J. L. Martinez-Hurtado, A. Garcia-Melendrez, F. Cruz Vasconcellos and C. R. Lowe, "A smartphone algorithm with inter-phone repeatability for the analysis of colorimetric tests," *Sensors and Actuators B: Chemical,* vol. 196, pp. 156-160, 2014.

[26] V. Oncescu, D. O'Dell and D. Erickson, "Smartphone based health accessory for colorimetric detection of biomarkers in sweat and saliva," *Lab on a Chip,* vol. 13, pp. 3232-3238, 2013.

ACCEPTED MANUSCRIPT

[1] S. K. Vashist, P. B. Luppa, L. Y. Yeo, A. Ozcan and J. H. T. Luong, "Emerging technologies for next-generation point-of-care testing," *Trends in biotechnology,* vol. 33, pp. 692-705, 2015.

[2] S. Wang, X. Zhao, I. Khimji, R. Akbas, W. Qiu, D. Edwards, D. W. Cramer, B. Ye and U. Demirci, "Integration of cell phone imaging with microchip ELISA to detect ovarian cancer HE4 biomarker in urine at the point-of-care," *Lab on a Chip,* vol. 11, pp. 3411-3418, 2011.

[3] H. Zhu, I. Sencan, J. Wong, S. Dimitrov, D. Tseng, K. Nagashima and A. Ozcan, "Cost-effective and rapid blood analysis on a cell-phone," *Lab on a Chip,* vol. 13, pp. 1282-1288, 2013.

[4] N. R. Pollock, J. P. Rolland, S. Kumar, P. D. Beattie, S. Jain, F. Noubary, V. L. Wong, R. A. Pohlmann, U. S. Ryan and G. M. Whitesides, "A paper-based multiplexed transaminase test for low-cost, point-of-care liver function testing," *Science translational medicine,* vol. 4, pp. 152ra129--152ra129, 2012.

[5] H. Shafiee, S. Wang, F. Inci, M. Toy, T. J. Henrich, D. R. Kuritzkes and U. Demirci, "Emerging technologies for point-of-care management of HIV infection," *Annual review of medicine,* vol. 66, pp. 387-405, 2015.

[6] B. Veigas, J. M. Jacob, M. N. Costa, D. S. Santos, M. Viveiros, J. In{\'a}cio, R. Martins, P. Barquinha, E. Fortunato and P. V. Baptista, "Gold on paper--paper platform for Au-nanoprobe TB detection," *Lab on a Chip,* vol. 12, pp. 4802-4808, 2012.

[7] H. Zhu, O. Yaglidere, T.-W. Su, D. Tseng and A. Ozcan, "Cost-effective and compact wide-field fluorescent imaging on a cell-phone," *Lab on a Chip,* vol. 11, pp. 315-322, 2011.

[8] G.-H. Chen, W.-Y. Chen, Y.-C. Yen, C.-W. Wang, H.-T. Chang and C.-F. Chen, "Detection of mercury (II) ions using colorimetric gold nanoparticles on paper-based analytical devices," *Analytical chemistry,* vol. 86, pp. 6843-6849, 2014.

[9] Q. Wei, R. Nagi, K. Sadeghi, S. Feng, E. Yan, S. J. Ki, R. Caire, D. Tseng and A. Ozcan, "Detection and spatial mapping of mercury contamination in water samples using a smart-phone," *ACS nano,* vol. 8, pp. 1121-1129, 2014.

[10] S. Sumriddetchkajorn, K. Chaitavon and Y. Intaravanne, "Mobile device-based self-referencing colorimeter for monitoring chlorine concentration in water," *Sensors and Actuators B: Chemical,* vol. 182, pp. 592-597, 2013.

[11] M. O. Salles, G. N. Meloni, W. R. Araujo and T. R. L. C. Paixao, "Explosive colorimetric discrimination using a smartphone, paper device and chemometrical approach," *Analytical Methods,* vol. 6, pp. 2047-2052, 2014.

[12] C. M. McGeough and S. O'Driscoll, "Camera phone-based quantitative analysis of C-reactive protein ELISA," *IEEE transactions on biomedical circuits and systems,* vol. 7, pp. 655-659, 2013.

[13] A. J. S. McGonigle, T. C. Wilkes, T. D. Pering, J. R. Willmott, J. M. Cook, F. M. Mims and A. V. Parisi, "Smartphone Spectrometers," *Sensors,* vol. 18, p. 223, 2018.

[14] R. C. Murdock, L. Shen, D. K. Griffin, N. Kelley-Loughnane, I. Papautsky and J. A. Hagen, "Optimization of a paper-based ELISA for a human performance biomarker," *Analytical chemistry,* vol. 85, pp. 11634-11642, 2013.

ACCEPTED MANUSCRIPT

[15] T. Ogirala, A. Eapen, K. G. Salvante, T. Rapaport, P. A. Nepomnaschy and A. M. Parameswaran, "Smartphone-based colorimetric ELISA implementation for determination of women's reproductive steroid hormone profiles," *Medical \& biological engineering \& computing,* vol. 55, pp. 1735-1741, 2017.

[16] B. Berg, B. Cortazar, D. Tseng, H. Ozkan, S. Feng, Q. Wei, R. Y.-L. Chan, J. Burbano, Q. Farooqui, M. Lewinski and others, "Cellphone-based hand-held microplate reader for point-of-care testing of enzyme-linked immunosorbent assays," *ACS nano,* vol. 9, pp. 7857-7866, 2015.

[17] J. M. Bland and D. G. Altman, "Comparing methods of measurement: why plotting difference against standard method is misleading," *The lancet,* vol. 346, pp. 1085-1087, 1995.

[18] S. C. Kim, U. M. Jalal, S. B. Im, S. Ko and J. S. Shim, "A smartphone-based optical platform for colorimetric analysis of microfluidic device," *Sensors and Actuators B: Chemical,* vol. 239, pp. 52-59, 2017.

[19] L. Shen, J. A. Hagen and I. Papautsky, "Point-of-care colorimetric detection with a smartphone," *Lab on a Chip,* vol. 12, pp. 4240-4243, 2012.

[20] K. E. McCracken and J.-Y. Yoon, "Recent approaches for optical smartphone sensing in resource-limited settings: a brief review," *Analytical Methods,* vol. 8, pp. 6591-6601, 2016.

[21] A. Roda, E. Michelini, M. Zangheri, M. Di Fusco, D. Calabria and P. Simoni, "Smartphone-based biosensors: A critical review and perspectives," *TrAC Trends in Analytical Chemistry,* vol. 79, pp. 317-325, 2016.

[22] O. Mudanyali, S. Dimitrov, U. Sikora, S. Padmanabhan, I. Navruz and A. Ozcan, "Integrated rapid-diagnostic-test reader platform on a cellphone," *Lab on a Chip,* vol. 12, pp. 2678-2686, 2012.

[23] S. K. Vashist, T. Oordt, E. M. Schneider, R. Zengerle, F. Stetten and J. H. T. Luong, "A smartphone-based colorimetric reader for bioanalytical applications using the screen-based bottom illumination provided by gadgets," *Biosensors and Bioelectronics,* vol. 67, pp. 248-255, 2015.

[24] S. Sumriddetchkajorn, K. Chaitavon and Y. Intaravanne, "Mobile-platform based colorimeter for monitoring chlorine concentration in water," *Sensors and Actuators B: Chemical,* vol. 191, pp. 561-566, 2014.

[25] A. K. Yetisen, J. L. Martinez-Hurtado, A. Garcia-Melendrez, F. Cruz Vasconcellos and C. R. Lowe, "A smartphone algorithm with inter-phone repeatability for the analysis of colorimetric tests," *Sensors and Actuators B: Chemical,* vol. 196, pp. 156-160, 2014.

[26] V. Oncescu, D. O'Dell and D. Erickson, "Smartphone based health accessory for colorimetric detection of biomarkers in sweat and saliva," *Lab on a Chip,* vol. 13, pp. 3232-3238, 2013.

[27] J. I. Hong and B.-Y. Chang, "Development of the smartphone-based colorimetry for multi-analyte sensing arrays," *Lab on a Chip,* vol. 14, pp. 1725-1732, 2014.

[28] S. T. Krauss, A. Q. Nauman, G. T. Garner and J. P. Landers, "Color manipulation through microchip tinting for colorimetric detection using hue image analysis," *Lab on a Chip,* vol. 17, pp. 4089-4096, 2017.

ACCEPTED MANUSCRIPT

[29] V. Oncescu, M. Mancuso and D. Erickson, "Cholesterol testing on a smartphone," *Lab on a Chip,* vol. 14, pp. 759-763, 2014.

[30] A. Battisti, P. Minei, A. Pucci and R. Bizzarri, "Hue-based quantification of mechanochromism towards a cost-effective detection of mechanical strain in polymer systems," *Chemical Communications,* vol. 53, pp. 248-251, 2017.

[31] K. E. McCracken, S. V. Angus, K. A. Reynolds and J.-Y. Yoon, "Multimodal imaging and lighting bias correction for improved μPAD-based water quality monitoring via smartphones," *Scientific reports,* vol. 6, p. 27529, 2016.

[32] N. L. Dell, S. Venkatachalam, D. Stevens, P. Yager and G. Borriello, "Towards a point-of-care diagnostic system: automated analysis of immunoassay test data on a cell phone," in *Proceedings of the 5th ACM workshop on Networked systems for developing regions*, 2011.

[33] J. L. Pech-Pacheco, G. Cristobal, J. Chamorro-Martinez and J. Fernandez-Valdivia, "Diatom autofocusing in brightfield microscopy: a comparative study," in *Pattern Recognition, 2000. Proceedings. 15th International Conference on*, 2000.

[34] S. K. Hanneman, "Design, analysis and interpretation of method-comparison studies," *AACN advanced critical care,* vol. 19, p. 223, 2008.

ACCEPTED MANUSCRIPT

ACCEPTED MANUSCRIPT

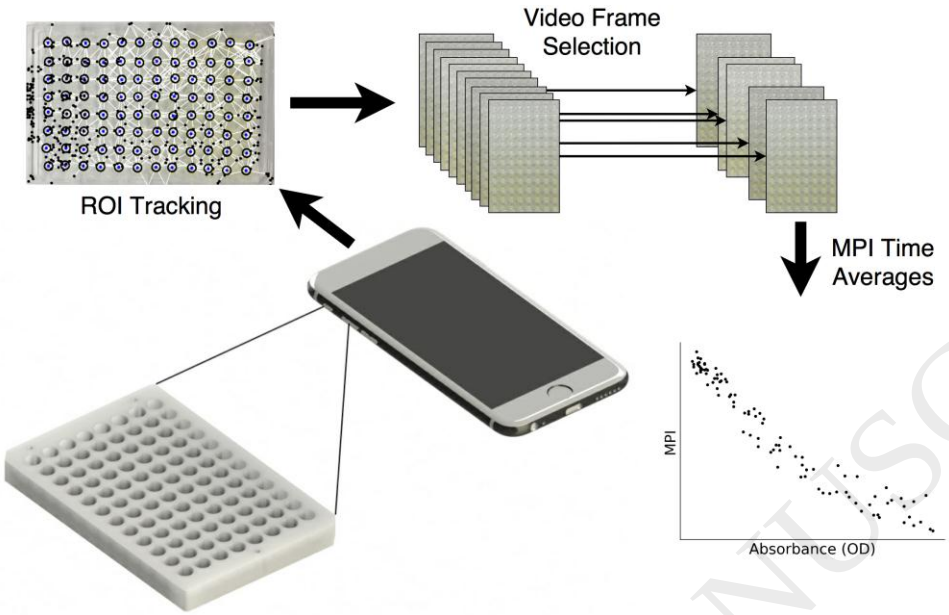

Figure 1: Schematic of our equipment-free video algorithm. Video frames are (1) captured by a smartphone above the 96 well plate, (2) input to the ROI tracking algorithm to follow the wells throughout the video, (3) classified using the image features, (4) input to the MPI method. The time averages of the MPIs from the selected frames are correlated with the absorbance measured via spectrophotometer.

ACCEPTED MANUSCRIPT

ACCEPTED MANUSCRIPT

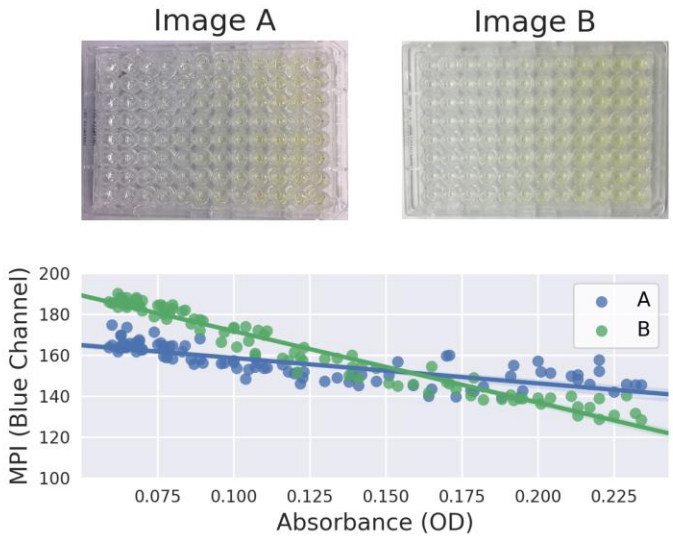

Figure 2: MPI analysis of two images taken under the same lighting conditions, with similar camera settings and position. Image A has R^2 = 0.60, standard error = 10, and a range of 36 MPI units. Image B has R^2 = 0.95, standard error = 8, and a range of 61 MPI units.

ACCEPTED MANUSCRIPT

ACCEPTED MANUSCRIPT

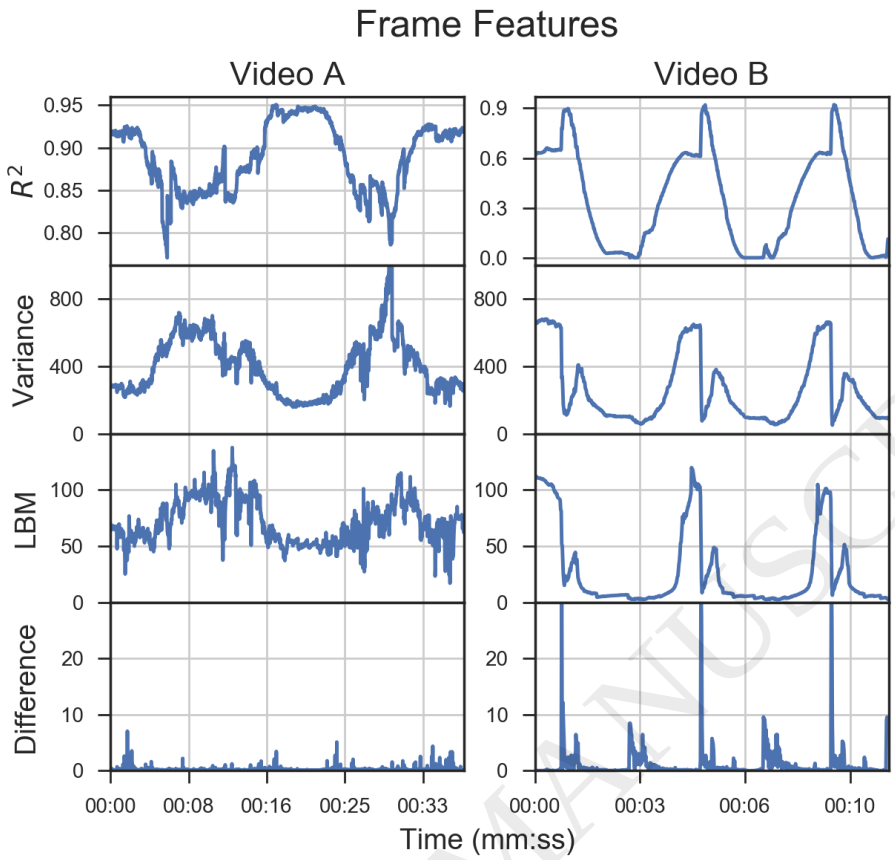

Figure 3: Image features over time for two smartphone videos. Video A was imaged at a variable distance to the liquid sample. The minimum separation distance was reached at 00:09 and 00:27, while the maximum distance was reached at 00:18. Video B was subjected to automatic white balance and blur at 00:01, 00:05, and 00:09.

ACCEPTED MANUSCRIPT

ACCEPTED MANUSCRIPT

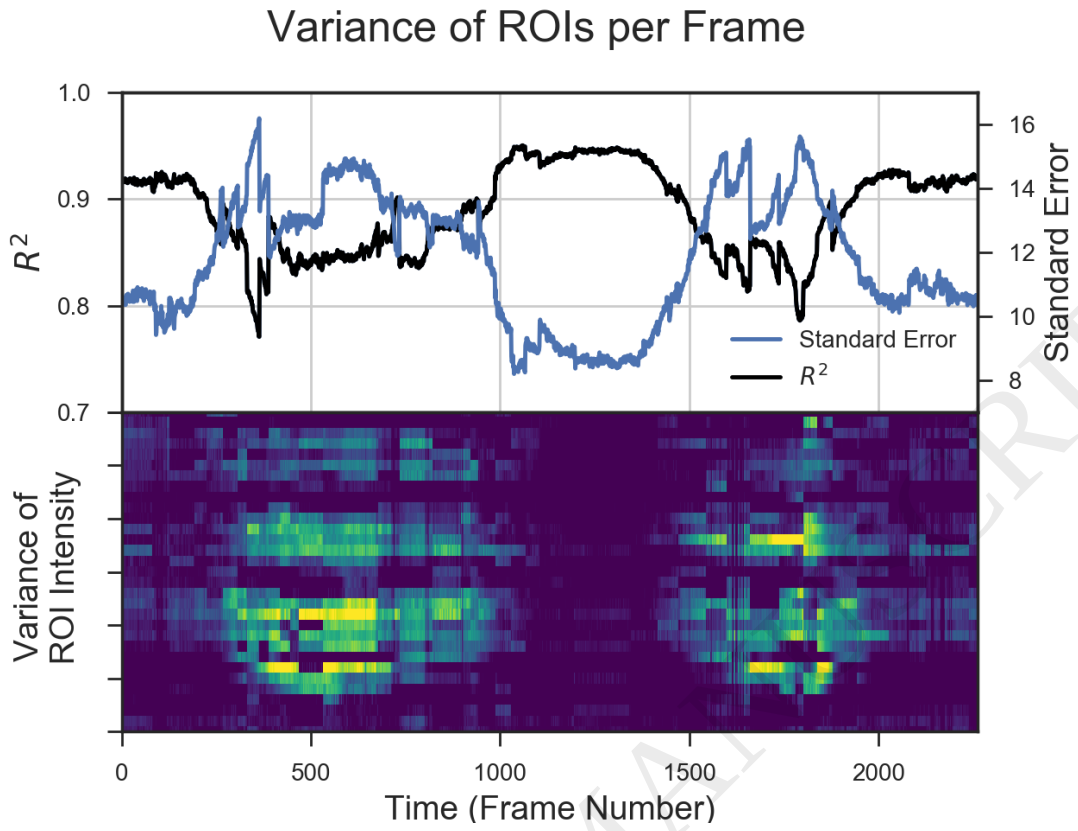

Figure 4: Relationship between ROI variance (bottom) and correlation (top). The bottom image shows the variances of the intensity histograms for the blue channel of the 96 ROIs. Variances are shown by pixel, where the row in the image corresponds to the well of the 96 well plate and the column corresponds to the video frame. Bright regions of the image indicate high variance histograms. In this video, the distance to the sample changed near t = 500 frames and t = 1750 frames.

ACCEPTED MANUSCRIPT

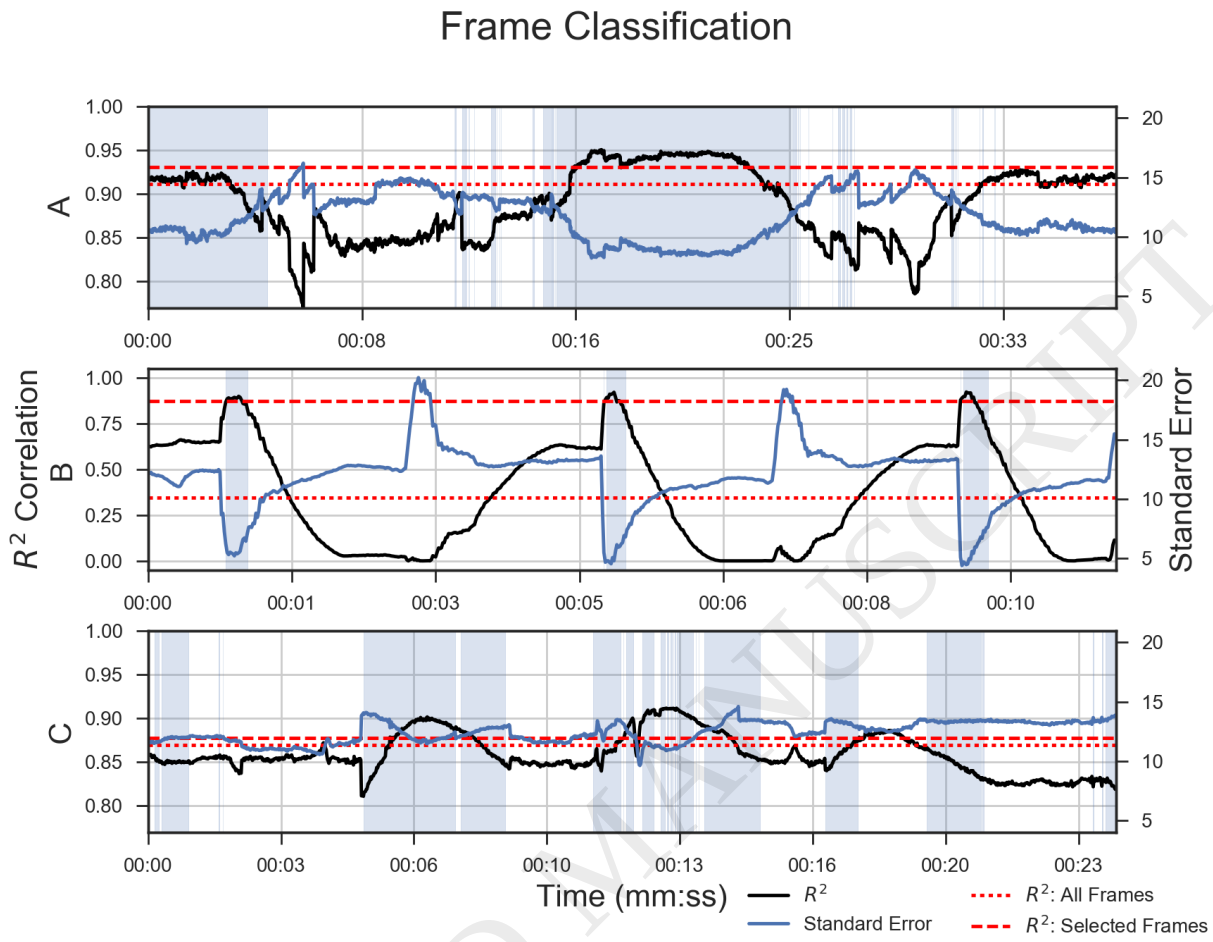

Figure 5: Frame classification results. Video A (top) was imaged with a variable distance to the sample. Video B (middle) was subjected to blur and white balance modifications. Video C (bottom) introduced a horizontal displacement at 00:10 and 00:21, causing the 96 well plate to be off center. Shaded regions of the plot indicate frames that were selected by the algorithm. The dashed red line indicates the R^2 of the time-averaged MPI from the selected frames. The dotted red line indicates the R^2 of all frames in the entire video. Note that all scales are standardized, except the R^2 scale for Video B.

ACCEPTED MANUSCRIPT

ACCEPTED MANUSCRIPT

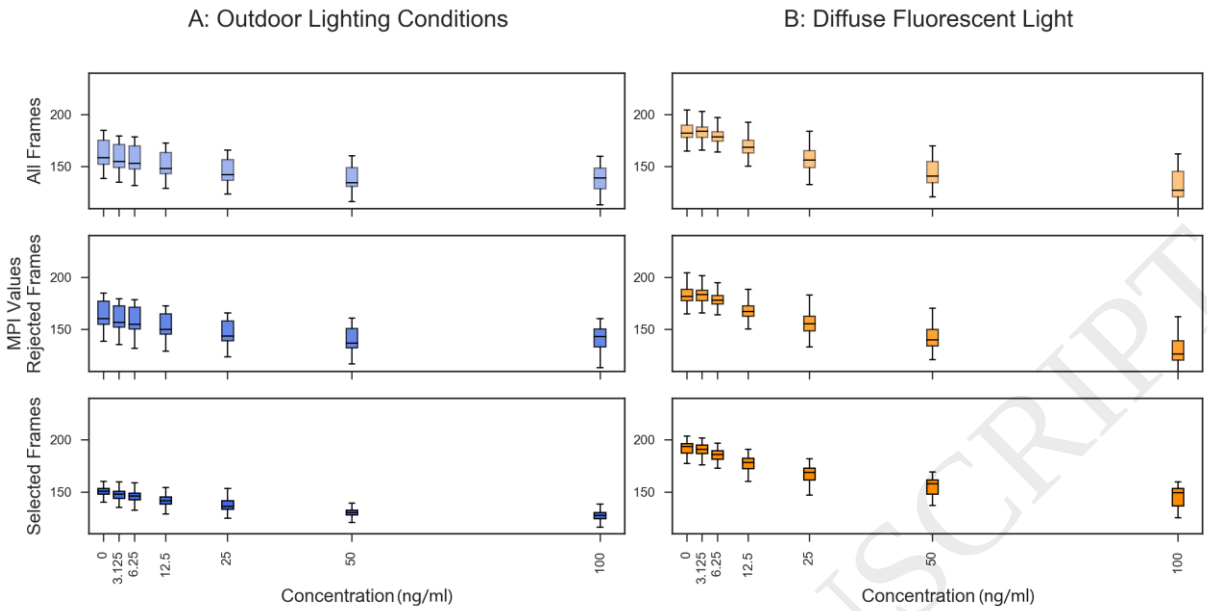

Figure 6: Standard MPI-concentration curve for (A) unpredictable outdoor lighting conditions and (B) diffuse indoor fluorescent lighting. Unpredictable lighting conditions result in a reduction in dynamic range and an increase in variance for each concentration value. For videos taken outdoors (A), the limit of detection was 35.5 ng/ml for all frames, 32.5 ng/ml for rejected frames, and 16 ng/ml for selected frames. For videos taken indoors (B), the limit of detection was 12.75 ng/ml for all frames, 13 ng/ml for rejected frames, and 10.5 ng/ml for selected frames. Absorbance values were also measured to estimate the selectivity of the method. In (A), the MPI-absorbance curve had $R^2 = 0.69$ and for (B) $R^2 = 0.75$.